Pion photoproduction on the deuteron: The reaction $\gamma d \to \pi^0 d$

H. Garcilazo
Escuela Superior de Física y Matemáticas, Instituto Politécnico Nacional, Edificio 9, Unidad Profesional "Adolfo Lopez Mateos," 07738 México D.F., Mexico

E. Moya de Guerra
Instituto de Estructura de la Materia, Consejo Superior de Investigaciones Científicas, Serrano 119, E-28006 Madrid, Spain
(Received 6 June 1994; revised manuscript received 21 March 1995)

We calculate the differential cross section, photon asymmetry, and initial deuteron polarizations of the reaction $\gamma d \to \pi^0 d$ in the energy region from threshold up to 1 GeV. We compare our results with available data and give predictions where no data are available. The calculation is performed fully relativistically, by applying the spectator-on-mass-shell prescription to the single- and double-scattering diagrams. We study the sensitivity of this reaction to the use of pseudovector versus pseudoscalar πNN couplings when the elementary $\gamma N \to \pi N$ reaction takes place on a bound nucleon.

PACS number(s): 25.20.−x, 21.45.+v, 13.60.Le

I. INTRODUCTION

Pion photoproduction on the deuteron can proceed in practice only through the reactions

$$\gamma d \to \pi^0 d \ , \tag{1a}$$
$$\gamma d \to \pi^0 np \ , \tag{1b}$$
$$\gamma d \to \pi^- pp \ , \tag{1c}$$
$$\gamma d \to \pi^+ nn \ , \tag{1d}$$

which are closely related to the processes

$$\pi^+ d \to \gamma pp \ , \tag{2a}$$
$$\pi^- d \to \gamma nn \ . \tag{2b}$$

Unfortunately, the reactions with an initial $\pi^0 d$ state are impossible from the experimental point of view due to the short lifetime of the neutral meson. Since the reaction (1a) is the only one that leads to a two-body final state, a relatively large amount of experimental data are available for it, while that is not the case for the reactions that end up with a three-body final state. Thus the reaction $\gamma d \to \pi^0 d$ is the logical first choice if one intends to study the pion photoproduction reactions in systems of more than one nucleon.

In a recent paper [1], we have constructed a model of pion photoproduction and electroproduction on the nucleon that describes this reaction qualitatively all the way from threshold up to 1 GeV and quantitatively up to 800 MeV. In this paper we apply the model of Ref. [1] to study the first of the pion photoproduction reactions on the deuteron. Some preliminary results have already been presented in Ref. [2]. The application of our model to the reactions leading to three-body final states will be presented elsewhere.

Previous studies of the $\gamma d \to \pi^0 d$ reaction [3–8] have been restricted to energies between threshold and the Δ resonance region. They have also been restricted to a nonrelativistic treatment, and in some cases very drastic approximations have been made such as the neglect of the effects of Fermi motion. Our treatment, on the other hand, is fully relativistic (within the spectator-on-mass-shell prescription), and we introduce approximations only in the higher-order rescattering term which is in general small except at threshold. We test the accuracy of our approximate formula for the double-scattering term, by calculating it exactly in the region near threshold, and find it to be quite reliable.

II. FORMALISM

We calculate the cross section and polarization observables of the process $\gamma d \to \pi^0 d$ by evaluating the Feynman diagrams depicted in Figs. 1(a) and 1(b) using the spectator-on-mass-shell prescription. Following the rules of Ref. [9], we write the differential cross section in the c.m. frame as

$$\frac{d\sigma}{d\Omega} = \frac{1}{64\pi^2 S} \frac{|\vec{q}|}{|\vec{k}|} \frac{1}{6} T_r \ , \tag{3}$$

where S is the invariant mass squared of the system, $\vec{q}$ and $\vec{k}$ are the c.m. momenta of the pion and photon, respectively, and the trace is given by

$$T_r = 2 \sum_{\lambda_i \lambda_f} |A_{\lambda_i \lambda_f}|^2 \ , \tag{4}$$

where $A_{\lambda_i \lambda_f}$ are the amplitudes of the $\gamma d \to \pi^0 d$ process corresponding to initial photon helicity $\lambda_\gamma = 1$ and λ_i and λ_f are, respectively, the initial and final helicities of the deuteron (the factor of 2 comes from the amplitudes corresponding to $\lambda_\gamma = -1$, which are of course related to those with $\lambda_\gamma = 1$ by parity conservation and time-reversal invariance). The initial state polarization

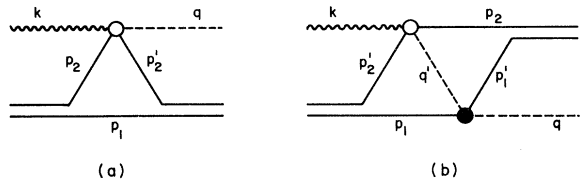

FIG. 1. $\gamma d \to \pi^0 d$ amplitude. (a) Single-scattering term. (b) Double-scattering term.

observables Σ (photon asymmetry), iT_{11} (vector analyzing power of the deuteron), and T_{20}, T_{21}, and T_{22} (tensor analyzing powers of the deuteron) are given in terms of the amplitudes of Eq. (4) by

$$\Sigma = \frac{4}{T_r}\mathrm{Re}[A^*_{11}A_{-1-1} - A^*_{10}A_{-10} + A^*_{1-1}A_{-11} - A^*_{01}A_{0-1} + |A_{00}|^2/2] , \quad (5)$$

$$iT_{11} = \frac{\sqrt{6}}{T_r}\mathrm{Im}[A^*_{0-1}A_{1-1} + A^*_{00}A_{10} + A^*_{01}A_{11} - A^*_{01}A_{-11} - A^*_{00}A_{-10} - A^*_{0-1}A_{-1-1}] , \quad (6)$$

$$T_{20} = \frac{\sqrt{2}}{T_r}[|A_{1-1}|^2 + |A_{10}|^2 + |A_{11}|^2 + |A_{-11}|^2 + |A_{-10}|^2 + |A_{-1-1}|^2 - 2(|A_{0-1}|^2 + |A_{00}|^2 + |A_{01}|^2)] , \quad (7)$$

$$T_{21} = -\frac{\sqrt{6}}{T_r}\mathrm{Re}[A^*_{0-1}A_{1-1} + A^*_{00}A_{10} + A^*_{01}A_{11} - A^*_{01}A_{-11} - A^*_{00}A_{-10} - A^*_{0-1}A_{-1-1}] , \quad (8)$$

$$T_{22} = \frac{2\sqrt{3}}{T_r}\mathrm{Re}[A^*_{-1-1}A_{1-1} + A^*_{-10}A_{10} + A^*_{-11}A_{11}] . \quad (9)$$

In what follows we describe our calculations of the amplitudes entering in Eqs. (3)–(9).

A. Spectator-on-mass-shell prescription

The contribution of the diagram of Fig. 1(a) to the amplitude A is given by (here in order to simplify the notation we suppress all the helicity indices)

$$A^{(a)} = \frac{1}{(2\pi)^4}\int d^4p_1(-V^\dagger_{dNN})i\frac{\not P - \not q - \not p_1 + M}{(P-q-p_1)^2 - M^2 + i\epsilon}t_{\gamma N\to\pi N}i\frac{\not p_1 + M}{p_1^2 - M^2 + i\epsilon}i\frac{\not P - \not k - \not p_1 + M}{(P-k-p_1)^2 - M^2 + i\epsilon}V_{dNN} , \quad (10)$$

where P is the total four-momentum, $t_{\gamma N\to\pi N}$ is the pion photoproduction amplitude on the nucleon, and V_{dNN} is the deuteron-nucleon-nucleon vertex.

We now integrate over the fourth component of the loop integration in Eq. (10) by using the spectator-on-mass-shell prescription [10]. That is, we integrate over the fourth component of the momentum p_1 in Eq. (10) by closing the contour from below and assuming that only the pole at $p_{10} = \sqrt{M^2 + \vec{p}_1^{\,2}} - i\epsilon \equiv E_1 - i\epsilon$ contributes to the integral so as to get

$$A^{(a)} = \frac{1}{(2\pi)^3}\int \frac{M}{E_1}d\vec{p}_1\bar{v}_1(\vec{p}_1)V^\dagger_{dNN}\frac{\not P - \not q - \not p_1 + M}{(P-q-p_1)^2 - M^2 + i\epsilon}t_{\gamma N\to\pi N}\frac{\not P - \not k - \not p_1 + M}{(P-k-p_1)^2 - M^2 + i\epsilon}V_{dNN}v_1(\vec{p}_1) , \quad (11)$$

where $v_1 = i\gamma_2 u_1^*$ is a charge conjugate spinor [9]. By using the same kind of manipulations, the amplitude corresponding to Fig. 1(b) can be written as

$$A^{(b)} = \frac{1}{(2\pi)^6}\int \frac{M}{E_1}d\vec{p}_1\frac{M}{E_2}d\vec{p}_2\bar{v}_2(\vec{p}_2)V^\dagger_{dNN}\frac{\not P - \not q - \not p_2 + M}{(P-q-p_2)^2 - M^2 + i\epsilon}t_{\pi N\to\pi N}u_1(\vec{p}_1) \times\frac{1}{(P-p_1-p_2)^2 - m^2 + i\epsilon}\bar{u}_2(\vec{p}_2)t_{\gamma N\to\pi N}\frac{\not P - \not k - \not p_1 + M}{(P-k-p_1)^2 - M^2 + i\epsilon}V_{dNN}v_1(\vec{p}_1) . \quad (12)$$

B. dNN vertex

In Eqs. (11) and (12), V_{dNN} is the dNN vertex with one nucleon on the mass shell (the spectator nucleon) and one nucleon off the mass shell (the exchanged nucleon). This vertex has the form [11–13]

$$V_{dNN} = F(p_2^2)\not\epsilon_d + \frac{1}{M}G(p_2^2)\epsilon_d\cdot p_1 + \frac{\not p_2 - M}{M}\left[H(p_2^2)\not\epsilon_d + \frac{1}{M}I(p_2^2)\epsilon_d\cdot p_1\right] , \quad (13)$$

where ϵ_d is the polarization vector of the deuteron and p_1 and p_2 are the four-momenta of the on-shell and off-shell nucleons, respectively. The form factors F, G, H, and I are related to the four components of the deuteron wave function, u, w, v_t, and v_s, where u and w are the usual upper components described by the $^3S_1$ and $^3D_1$ states and

v_t and v_s are the lower components described by the $^3P_1$ and $^1P_1$ states. As has been shown by Gross and co-workers [12,13], the connection between the form factors and the four components of the deuteron wave function is

$$F(p_2^2) = \pi\sqrt{2M_d}(2E - M_d)\left[u(p) - \frac{1}{\sqrt{2}}w(p) + \frac{M}{p}\sqrt{\frac{3}{2}}v_t(p)\right] , \tag{14}$$

$$G(p_2^2) = \pi\sqrt{2M_d}(2E - M_d)\left[\frac{M}{E+M}u(p) + \frac{M(2E+M)}{\sqrt{2}p^2}w(p) + \frac{M}{p}\sqrt{\frac{3}{2}}v_t(p)\right] , \tag{15}$$

$$H(p_2^2) = \pi\sqrt{2M_d}\frac{EM}{p}\sqrt{\frac{3}{2}}v_t(p) , \tag{16}$$

$$I(p_2^2) = -\pi\sqrt{2M_d}\frac{M^2}{M_d}\left\{(2E - M_d)\left[\frac{1}{E+M}u(p) - \frac{E+2M}{\sqrt{2}p^2}w(p)\right] + \frac{M_d}{p}\sqrt{3}v_s(p)\right\} , \tag{17}$$

where M_d is the mass of the deuteron, $E = \sqrt{p^2 + M^2}$, and p is the magnitude of the nucleon-nucleon relative three-momentum in the c.m. frame, which is a Lorentz invariant given by

$$p^2 = \frac{(M_d^2 + M^2 - p_2^2)^2}{4M_d^2} - M^2 . \tag{18}$$

The four components of the deuteron wave function are normalized such that

$$\int_0^\infty p^2 dp[u^2(p) + w^2(p) + v_t^2(p) + v_s^2(p)] = 1 . \tag{19}$$

The upper components u and w are well known from standard potential models. The lower components v_t and v_s, on the other hand, can only be obtained by using a theory that takes explicitly into account the negative-energy degrees of freedom of the nucleon that is going off mass shell. These lower components of the deuteron wave function have been studied extensively by Buck and Gross [13] within the framework of the Gross equation [14] in which one nucleon is always kept on mass shell. In their study, Buck and Gross [13] used a one-boson-exchange (OBE) model with π, ρ, ω, and σ exchange, where the main responsible for the coupling to the negative-energy states is the one-pion-exchange (OPE) term. Therefore, they used a πNN vertex which is a linear combination of pseudoscalar and pseudovector coupling as

$$V_{\pi NN} = \lambda g\gamma_5 + (1-\lambda)\frac{f}{m}\gamma_5 \not{q} , \tag{20}$$

where the case $\lambda = 1$ corresponds to pure pseudoscalar coupling, while the case $\lambda = 0$ corresponds to pure pseudovector coupling. Using the equivalence theorem [15], the pseudovector and pseudoscalar coupling constants are related as

$$f = \frac{m}{2M}g , \tag{21}$$

with m and M the pion and nucleon masses, respectively. Not surprisingly, Buck and Gross found that the strongest coupling to the negative-energy states is obtained with $\lambda = 1$. That this should be so follows from the structure of the vertices in Eq. (20).

In the study of Buck and Gross, a family of deuteron wave functions was constructed by considering $\lambda = 0.0$, 0.2, 0.4, 0.6, 0.8, and 1.0, where in each case the parameters of the OBE model were adjusted to reproduce the static properties of the deuteron (binding energy, quadrupole moment, magnetic moment, and asymptotic D/S ratio). Thus we will use their models in order to evaluate the amplitudes of the processes depicted in Figs. 1(a) and 1(b). As far as we know, this is the first calculation of the pion photoproduction reactions on the deuteron, where the lower components of the deuteron wave function have been explicitly taken into account.

C. Double-scattering term

Since the contribution of the double-scattering term given by Eq. (12) is know to be much smaller than the single-scattering term as one goes away from threshold [3], we will calculate this amplitude using an approximate formula. At threshold, however, where the sixfold integration in Eq. (12) simplifies considerably, we evaluate it exactly in order to test how good our approximate formula is. The latter is obtained as follows. First we notice from Fig. 1(b) and Eq. (12) that

$$p_2' = P - k - p_1 , \tag{22}$$

$$p_1' = P - q - p_2 , \tag{23}$$

$$q' = P - p_1 - p_2 . \tag{24}$$

Therefore, if we decompose the propagators of the exchanged nucleons into their two possible time orderings

and keep only the forward-going part, i.e.,

$$\frac{\not p'_2 + M}{p'^2_2 - M^2 + i\epsilon} \approx \frac{M}{E'_2}\frac{1}{p'_{20} - E'_2 + i\epsilon} u'_2(\vec{p}\,'_2)\bar{u}'_2(\vec{p}\,'_2) \ , \quad (25)$$

$$\frac{\not p'_1 + M}{p'^2_1 - M^2 + i\epsilon} \approx \frac{M}{E'_1}\frac{1}{p'_{10} - E'_1 + i\epsilon} u'_1(\vec{p}\,'_1)\bar{u}'_1(\vec{p}\,'_1) \ , \quad (26)$$

we can write Eq. (12) as

$$A^{(b)} = \frac{1}{(2\pi)^6}\int \frac{M}{E_1}d\vec{p}_1 \frac{M}{E_2}d\vec{p}_2 \psi^*_d(\vec{p}_f)\bar{u}'_1(\vec{p}\,'_1)t_{\pi N\to\pi N}u_1(\vec{p}_1)\frac{1}{q'^2 - m^2 + i\epsilon}\bar{u}_2(\vec{p}_2)t_{\gamma N\to\pi N}u'_2(\vec{p}\,'_2)\psi_d(\vec{p}_i) \ , \quad (27)$$

where

$$\psi_d(\vec{p}_i) = \frac{M}{E'_2}\frac{1}{p'_{20} - E'_2 + i\epsilon}\bar{u}'_2(\vec{p}\,'_2)V_{dNN}v_1(\vec{p}_1) \ , \quad (28)$$

$$\psi^*_d(\vec{p}_f) = \frac{M}{E'_1}\frac{1}{p'_{10} - E'_1 + i\epsilon}\bar{v}_2(\vec{p}_2)V^\dagger_{dNN}u'_1(\vec{p}\,'_1) \quad (29)$$

are the initial and final deuteron wave functions which depend on the initial and final relative momenta in the deuteron's rest frame $\vec{p}_i$ and $\vec{p}_f$. Since the deuteron wave function $\psi_d(\vec{p})$ peaks very strongly when $\vec{p} = \vec{0}$, the main contribution to the integral comes from the configuration where the kinematics of the double-scattering term is as shown in Fig. 2. Therefore, we can evaluate the $\pi N \to \pi N$ and $\gamma N \to \pi N$ t matrices at the kinematics of Fig. 2 and take them out of the integral. We thus get

$$A^{(b)} \approx \bar{u}'_1 t_{\pi N\to\pi N}u_1\bar{u}_2 t_{\gamma N\to\pi N}u'_2\frac{1}{(2\pi)^6}\int \frac{M}{E_1}d\vec{p}_1\frac{M}{E_2}d\vec{p}_2\psi^*_d(\vec{p}_f)\frac{1}{(\sqrt{S} - E_1 - E_2)^2 - (\vec{p}_1 + \vec{p}_2)^2 - m^2 + i\epsilon}\psi_d(\vec{p}_i) \ , \quad (30)$$

with $\psi_d(\vec{p}_i)$ and $\psi^*_d(\vec{p}_f)$ given by Eqs. (28) and (29). Notice that in the kinematics of Fig. 2, which is used to evaluate the $\pi N \to \pi N$ and $\gamma N \to \pi N$ t matrices, the fourth components of all the particles are completely determined due to the fact that the two spectator nucleons are on mass shell. In particular, as a consequence of the smallness of the deuteron's binding energy, the two exchanged nucleons are almost on mass shell. The propagator of the pion which appears inside the integral in Eqs. (27) and (30) contains singularities at $\sqrt{S} = E_1 + E_2 \pm E_{\pi'}$. The singularity at $\sqrt{S} = E_1 + E_2 + E_{\pi'}$ is well known, and it arises due to the fact that we can have an intermediate πNN state with all three particles on the mass shell. The singularity of $\sqrt{S} = E_1 + E_2 - E_{\pi'}$, on the other hand, is unphysical and it arises as a consequence of the spectator-on-mass-shell approximation [10]. This unphysical singularity gives rise to a logarithmic singularity after integrating over the angles. Since this logarithmic singularity appears at very high momenta $|\vec{p}_1|$ and $|\vec{p}_2|$, it will be avoided by integrating $|\vec{p}_1|$ and $|\vec{p}_2|$ from 0 up to 0.1 fm^{-1} before the singularity.

D. $\pi N \to \pi N$ amplitude

The $\pi N \to \pi N$ t matrix is needed only for the evaluation of the double-scattering term, which in general is very small; therefore, we have constructed a simple phenomenological model for it. We write the pion-nucleon amplitude for a given isospin channel I as a sum of projection operators for the various angular momentum channels as

$$t^I_{\pi N\to\pi N} = f^I_0(s)(\not P + \sqrt{s}) + f^I_1(s)(\not P - \sqrt{s}) + h^I_1(s)(\not P + \sqrt{s})\left[-q\cdot q' + \frac{\not q\,\not q'}{3} + \frac{2P\cdot qP\cdot q'}{3s} - \frac{P\cdot q\,\not q' - \not qP\cdot q'}{3\sqrt{s}}\right]$$
$$+h^I_2(s)(\not P - \sqrt{s})\left[-q\cdot q' + \frac{\not q\,\not q'}{3} + \frac{2P\cdot qP\cdot q'}{3s} + \frac{P\cdot q\,\not q' - \not qP\cdot q'}{3\sqrt{s}}\right] \ , \quad (31)$$

where $P = p_1 + q' = p'_1 + q$ is the pion-nucleon total momentum in the notation of Fig. 1(b) and $s = P^2$.

If one evaluates $\bar{u}'_1 t^I_{\pi N\to\pi N}u_1$ in the pion-nucleon c.m. frame, the first two terms in Eq. (31) generate the scattering amplitude with $j = 1/2$ for $l = 0$ and $l = 1$, respectively, while the last two terms generate the scattering amplitude with $j = 3/2$ for $l = 1$ and $l = 2$, respectively. Therefore, the functions f^I_0, f^I_1, h^I_1, and h^I_2 are directly related to the corresponding partial-wave

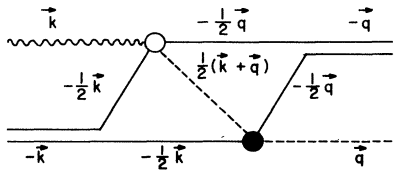

FIG. 2. Kinematics used in the evaluation of the double-scattering term with the approximate formula (30).

scattering amplitudes of each channel as

$$f_0^I(s) = -\frac{4\pi}{E+M}\frac{1}{2ip}[\eta_0^I(s)e^{2i\delta_0^I(s)} - 1] , \quad (32)$$

$$f_1^I(s) = -4\pi(E+M)\frac{1}{2ip^3}[\eta_1^I(s)e^{2i\delta_1^I(s)} - 1] , \quad (33)$$

$$h_1^I(s) = -\frac{12\pi}{E+M}\frac{1}{2ip^3}[\eta_1^I(s)e^{2i\delta_1^I(s)} - 1] , \quad (34)$$

$$h_2^I(s) = -12\pi(E+M)\frac{1}{2ip^5}[\eta_2^I(s)e^{2i\delta_2^I(s)} - 1] , \quad (35)$$

with

$$E = \sqrt{p^2+M^2} , \quad (36)$$

$$p^2 = \frac{1}{4s}[s-(M+m)^2][s-(M-m)^2] . \quad (37)$$

Since Eq. (31) is manifestly covariant, it can be used in any reference frame as well as in the case when any of the initial or final particles are off the mass shell.

Finally, taking into account the isospin structure of the deuteron, the product of amplitudes $t_{\pi N\to\pi N}t_{\gamma N\to\pi N}$ that enters into Eq. (30) is written explicitly as

$$t_{\pi N\to\pi N}t_{\gamma N\to\pi N}$$

$$= t_{\pi^0 p\to\pi^0 p}t_{\gamma p\to\pi^0 p} + t_{\pi^0 n\to\pi^0 n}t_{\gamma n\to\pi^0 n} - t_{\pi^+ n\to\pi^0 p}t_{\gamma p\to\pi^+ n} - t_{\pi^- p\to\pi^0 n}t_{\gamma n\to\pi^- p} . \quad (38)$$

E. $\gamma N \to \pi N$ amplitude

The $\gamma N \to \pi N$ amplitude is needed in the evaluation of both the single- and double-scattering terms. Our model of the $\gamma N \to \pi N$ amplitude has been discussed in detail in Ref. [1] and is shown diagrammatically in Fig. 3. It consists of the Born terms [Figs. 3(a)–3(d)], the t-channel contribution of the vector mesons ρ and ω [Fig. 3(e)], and the s- and u-channel contributions of the nucleon resonances P_{33}, P_{11}, S_{11}, S_{31}, D_{13}, and D_{33}. The γNN^* and πNN^* vertices were constructed considering all the possible couplings consistent with gauge invariance and satisfying the requirements of parity, spin, and isospin assignments for each resonance. In the case of spin-3/2 resonances, the vertices V_μ are required to satisfy the subsidiary condition

$$\gamma^\mu V_\mu = 0 , \quad (39)$$

in order to guarantee coupling to the pure spin-3/2 component of the Rarita-Schwinger propagator [16,17]. Once the vertices had been constructed, the πNN^* coupling constants were determined from the decay widths $N^* \to \pi N$. The γNN^* coupling constants, on the other hand, were obtained from the well-known resonance couplings obtained from $\gamma N \to \pi N$ partial-wave analyses [18,19]. We refer the reader to Ref. [1] for the precise form of the vertices and the values of the various coupling constants.

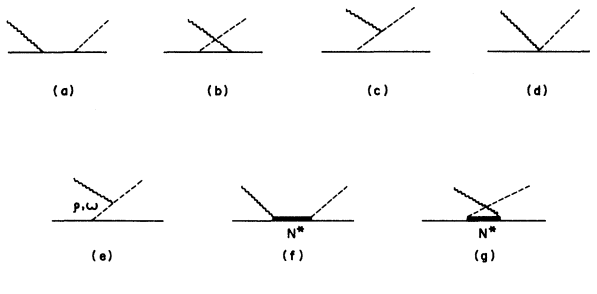

FIG. 3. Elementary $\gamma N \to \pi N$ amplitude. (a)–(d) Born terms. (e) Vector meson terms. (f) and (g) direct and crossed resonance terms. N^* stands for the P_{33}, P_{11}, S_{11}, S_{31}, D_{13}, D_{33} resonances.

It was found in Ref. [1] that at high energy the crossed resonance diagrams depicted in Fig. 3(g) give rise to a much too large contribution to the amplitude which in general tends to spoil the agreement with data. Therefore, it was necessary to regularize these diagrams by means of a cutoff of the form

$$g(p^2) = \frac{\Lambda^2}{\Lambda^2+p^2} , \quad (40)$$

where p^2 is the magnitude of the pion-nucleon relative three-momentum squared given by Eq. (37) and $\Lambda = 300$ MeV/c.

An important modification made here of the model of Ref. [1] concerns the form of the πNN vertex used in the evaluation of the Born diagrams [Figs. 3(a)–3(d)]. In Ref. [1] we used pure pseudovector coupling [$\lambda = 0$ in Eq. (20)]. However, as we have discussed above, the deuteron wave functions used in the dNN vertex have been obtained with the πNN vertex of Eq. (20) which is a linear combination of pseudoscalar and pseudovector couplings. Therefore, in order to be consistent with the deuteron wave functions, we use also the same linear combination of pseudoscalar and pseudovector couplings given by Eq. (20) in the evaluation of the Born diagrams,

$$M_{\rm Born} = \lambda M_{\rm Born}^{\rm PS} + (1-\lambda)M_{\rm Born}^{\rm PV} . \quad (41)$$

The contact term in the case of pseudovector coupling arises naturally from the principle of minimal coupling [17]. In the case of pseudoscalar coupling, on the other hand, the contact term arises only as a consequence of chiral symmetry [20,21]. As discussed in Refs. [20,21], if one starts with the Lagrangian appropriate to pseudovector (PV) coupling, one ends up with the Lagrangian appropriate to pseudoscalar (PS) coupling by performing a chiral transformation.

The $\gamma N \to \pi N$ amplitude is written as

$$M = \chi_2^\dagger \sum_i \pi_i\{A^0\tau_i + A^-\tfrac{1}{2}[\tau_i,\tau_3] + A^+\delta_{i,3}\}\chi_1 , \quad (42)$$

where A^0, A^-, and A^+ are the dynamical amplitudes for the various isospin terms. The contact term in the case of pseudovector coupling gives a contribution to the dynamical amplitudes of

$$A^- = -\frac{f}{m}\bar{u}_2 \not{\epsilon}\gamma_5 u_1 \ , \tag{43a}$$

$$A^0 = 0 \ , \tag{43b}$$

$$A^+ = 0 \ , \tag{43c}$$

while the requirement of chiral invariance, in the case of pseudoscalar coupling, leads to a contribution from the contact term to the dynamical amplitudes of

$$A^- = 0 \ , \tag{44a}$$

$$A^0 = \frac{g}{(2M)^2}(\kappa_p + \kappa_n)\bar{u}_2 \not{\epsilon}\not{k}\gamma_5 u_1 \ , \tag{44b}$$

$$A^+ = \frac{g}{(2M)^2}(\kappa_p - \kappa_n)\bar{u}_2 \not{\epsilon}\not{k}\gamma_5 u_1 \ . \tag{44c}$$

Therefore, when we use the πNN vertex given in Eq. (20), the contribution from the diagram of Fig. 3(d) to the dynamical amplitudes is

$$A_d^- = -(1-\lambda)\frac{f}{m}\bar{u}_2 \not{\epsilon}\gamma_5 u_1 \ , \tag{45}$$

$$A_d^0 = \lambda\frac{g}{(2M)^2}(\kappa_p + \kappa_n)\bar{u}_2 \not{\epsilon}\not{k}\gamma_5 u_1 \ , \tag{46}$$

$$A_d^+ = \lambda\frac{g}{(2M)^2}(\kappa_p - \kappa_n)\bar{u}_2 \not{\epsilon}\not{k}\gamma_5 u_1 \ , \tag{47}$$

with f and g related by Eq. (21). ϵ and k are the photon's polarization vector and four-momentum, while $\kappa_p = 1.79$ and $\kappa_n = -1.91$ are the anomalous magnetic moments of the proton and neutron, respectively.

The $\gamma N \to \pi N$ amplitude (41) with the contribution of the contact term given by Eqs. (45)–(47) is independent of the value of λ in the case of a free nucleon. It is therefore very interesting to investigate this chiral invariance in the case when the nucleon is bound inside the deuteron. As we will see later, chiral invariance is broken for bound nucleons.

Finally, we should mention that the contribution of the diagram of Fig. 3(a) to the process of Fig. 1(a) generates the diagram depicted in Fig. 4. This diagram contains a pole due to the fact that the processes $\gamma d \to NN$ and $NN \to \pi d$ are both open channels even at threshold. Therefore, the numerical integration must be designed to take into account accurately this pole. This pole gives rise to an imaginary contribution to the diagram of Fig. 1(a) even at threshold as required by unitarity. Actually, at the pion threshold the diagram of Fig. 1(a) would be real if it were not for this contribution.

III. RESULTS

A. Accuracy of the double-scattering formula

Before presenting our results and their comparison with the data, it is important to discuss the reliability of our approximate formula for the double-scattering term given by Eq. (30). For this purpose, we considered the region very near threshold where the calculation simplifies considerably. In this region, the pion-nucleon scattering amplitude (31) is determined by the S wave alone, i.e., the first term in Eq. (31). Then

$$t^I_{\pi N\to\pi N} \approx -\frac{4\pi}{2M}a^I(\not{P} + \sqrt{s}) \ , \tag{48}$$

where a^I is the corresponding pion-nucleon scattering length. If we now take into account the isospin structure of the $\gamma N \to \pi N$ amplitude given by Eq. (42), we get, for the sum of terms in Eq. (38),

$$t_{\pi^0 p\to\pi^0 p}t_{\gamma p\to\pi^0 p} + t_{\pi^0 n\to\pi^0 n}t_{\gamma n\to\pi^0 n}$$

$$= -\frac{4\pi}{3M}(\not{P} + \sqrt{s})(2a^{3/2} + a^{1/2})A^+ \ , \tag{49}$$

$$-t_{\pi^+ n\to\pi^0 p}t_{\gamma p\to\pi^+ n} - t_{\pi^- p\to\pi^0 n}t_{\gamma n\to\pi^- p}$$

$$= \frac{4\pi}{3M}(\not{P} + \sqrt{s})(a^{3/2} - a^{1/2})A^- \ . \tag{50}$$

If we now use the fact that the pion-nucleon scattering lengths satisfy $2a^{3/2} + a^{1/2} \approx 0$, the contribution of Eq. (49) is negligible and we need to consider only the contribution of the charge-exchange processes given by Eq. (50). Moreover, since the charged pions are heavier than the neutral pion by about 5 MeV and the deuteron's binding energy is about 2 MeV, the three-body singularities of the double-scattering term start to create problems at only approximately 7 MeV above threshold (more precisely at $\omega = 147.1$ MeV) so that below this energy the integration in Eqs. (27) and (30) is free of three-body singularities. Also at threshold the diagrams of Figs. 3(c) and 3(d) are exactly zero for the amplitude A^- that enters into Eq. (50), while the vector mesons do not contribute to A^-. Finally, the contribution of the nucleon resonances is very small at threshold [1] so that they can be safely neglected. Thus the calculation of the double-scattering term simplifies enormously at threshold. We calculated the double-scattering term using both the exact expression (27) and the approximate formula (30) using $\lambda = 1$ in Eq. (20). As an example, we show in Table I the results for $\omega = 145$ MeV and $\theta_\pi = 75°$ for the nine independent helicity amplitudes that appear in Eqs. (4)–(9). As seen in Table I, the accuracy of our

TABLE I. Accuracy of the approximate formula for the double-scattering term given by Eq. (30) as compared with the exact result given by Eq. (27) for $\omega = 145$ MeV and $\theta_\pi = 75°$.

	A_{-1-1}	A_{-10}	A_{-11}	A_{0-1}	A_{00}	A_{01}	A_{1-1}	A_{10}	A_{11}
Exact	−0.001	0.116	−0.121	−0.001	0.122	0.047	−0.001	0.064	0.115
Approx.	−0.003	0.113	−0.119	−0.003	0.117	0.049	−0.002	0.060	0.113

approximate formula is about 5%.

We found that the results of the double-scattering term produced by our approximate formula (30) are essentially independent of the value of λ used in the πNN vertex (20). This is due to the fact that in the double-scattering term, as already mentioned, the two exchanged nucleons and the two spectator nucleons are almost exactly on the mass shell due to the spectator-on-mass-shell approximation and to the deuteron wave function. Therefore, only the intermediate pion in the double scattering term is off the mass shell, which has no effect at all with regard to the structure of the vertex.

B. Threshold region

The most complete calculation of the $\gamma d \to \pi^0 d$ reaction existing in the literature are those of Bosted and Laget [4] who used for the $\gamma N \to \pi N$ amplitude the Blomqvist-Laget model [22], which is a nonrelativistic reduction of the relativistic model of Olsson and Osypowski [23]. They evaluated also the single- and double-scattering terms within a nonrelativistic framework (although keeping relativistic kinematics for the pion propagator). Since the model of Refs. [4,22] is based in a πNN vertex with pseudovector coupling, it should correspond approximately to our model with $\lambda = 0$ in Eq. (20).

We show in Fig. 4 the results for the reduced cross section near threshold (threshold lies at 139.8 MeV) using only the single-scattering term. The short-dashed line is the result of pure pseudovector coupling [$\lambda = 0$ in Eq. (20)], and the solid line is the result of pure pseudoscalar coupling [$\lambda = 1$ in Eq. (20)], while the dashed and long-dashed curves correspond to $\lambda = 0.2$ and $\lambda = 0.6$, respectively. The most interesting feature of this figure is the strong sensitivity with respect to the form of the πNN vertex given in Eq. (20). Very close to threshold the results of $\lambda = 0$ and $\lambda = 1$ differ by more than one order of magnitude. Our results for pure pseudovector coupling are in good agreement with the corresponding ones of Bosted and Laget shown in Fig. 9

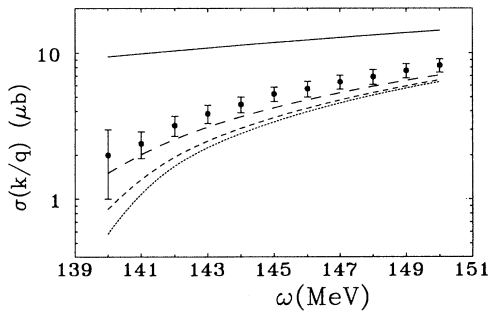

FIG. 4. Reduced cross sections of the $\gamma d \to \pi^0 d$ reaction near threshold calculated using only the single-scattering term. The short-dashed line corresponds to the model with $\lambda = 0$ in Eq. (20), the dashed line to $\lambda = 0.2$, the long-dashed line to $\lambda = 0.6$, and the solid line to $\lambda = 1$. Data are from Ref. [24].

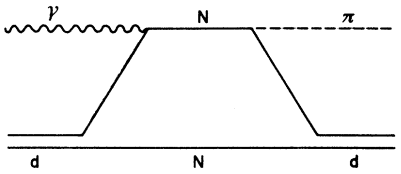

FIG. 5. Lowest-order contribution of the intermediate NN state to the reaction $\gamma d \to \pi^0 d$.

of Ref. [4]. The strong sensitivity of our results with respect to the form of the πNN vertex can be understood by considering the contribution of the pole term shown in Fig. 5, which is very important. This pole gives rise to an imaginary part for the amplitude $A^{(a)}$ given by Eq. (11), which at threshold is proportional to

$$\int d\hat{p}_1 F_{NN\to\pi d} F_{\gamma d\to NN} , \tag{51}$$

where the πNN vertex enters only in the $NN \to \pi d$ amplitude as indicated in Fig. 5. Moreover, at the pion threshold the modulus of the $NN \to \pi d$ amplitude is isotropic so that it enters in Eq. (51) essentially as a multiplicative constant. Thus, at threshold, if we study the sensitivity of the $NN \to \pi d$ amplitude with respect to the form of the πNN vertex, this determines also the sensitivity of $\mathrm{Im}A^{(a)}$ on the πNN vertex. We have calculated the two independent amplitudes f_p and f_a of the

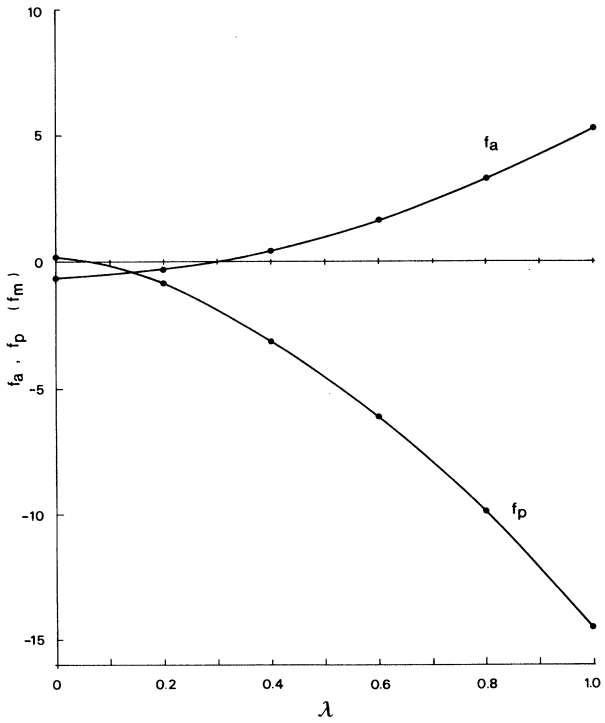

FIG. 6. Two independent amplitudes f_p and f_a of the $NN \to \pi d$ amplitude at threshold (see text) as functions of the parameter λ of Eq. (20).

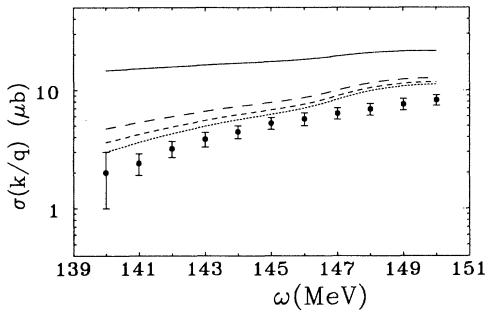

FIG. 7. Reduced cross sections of the $\gamma d \to \pi^0 d$ reaction near threshold calculated using both the single- and double-scattering terms. The meaning of the curves is the same as in Fig. 5. Data are from Ref. [24].

process $NN \to \pi d$ in the forward direction that correspond, respectively, to the spins of the two nucleons being parallel or antiparallel. As mentioned before, these amplitudes are essentially isotropic. We show in Fig. 6 the two amplitudes f_p and f_a as functions of the parameter λ of Eq. (20). As seen in this figure, both amplitudes are approximately 0 for $\lambda = 0$ and become very large when λ approaches 1, that is, when the vertex becomes pure pseudoscalar.

We show in Fig. 7 the results for the reduced cross section when we include both the single- and double-scattering terms. As one sees, for pure pseudovector coupling the reduced cross section at 140 MeV changes from 0.55 to 3 μb due to the double-scattering term. The fact that the double-scattering term is very important in the threshold region is well known [4–8] and is due to an accidental cancellation of the elementary $\gamma N \to \pi^0 N$ amplitude at threshold. Our results for pure pseudovector coupling when we include the double-scattering term are about 20% larger than the corresponding results of Bosted and Laget [4]. However, they are about 20% smaller than the corresponding results of Koch and Woloshyn [8]. The theoretical results for all values of λ lie above the data. The fact that there is disagreement between theory and data is not so surprising, since the importance of the double-scattering term tells us that also the third- and higher-order scattering terms are not negligible at threshold. Thus, in order to be able to understand the experimental results at threshold, one would have to perform a full three-body calculation of the final state.

C. First resonance region

We show in Fig. 8 our results for the differential cross section at energies in the region of the first resonance. The short-dashed, dashed, long-dashed, and solid curves correspond, respectively, to the models with $\lambda = 0$, 0.6, 0.8, and 1. As the energy increases, the region of large angles clearly seems to favor the models with λ large. At these energies the double-scattering term has an effect

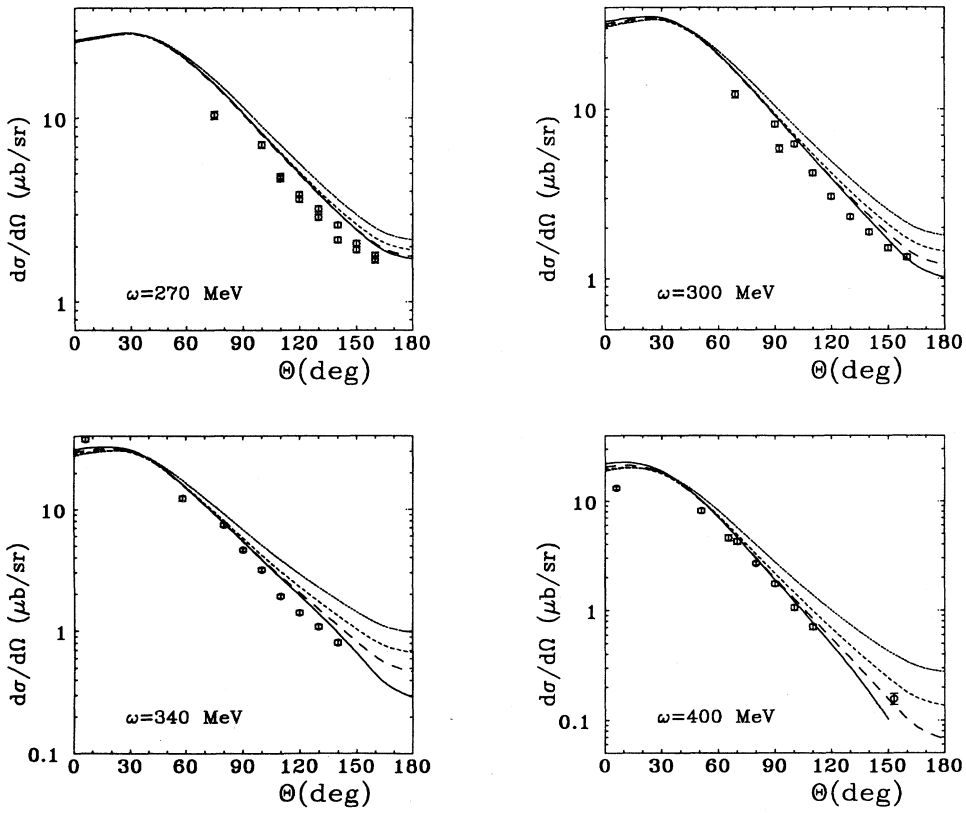

FIG. 8. Differential cross sections of the $\gamma d \to \pi^0 d$ reaction at 270, 300, 340, and 400 MeV. The short-dashed line corresponds to the model with $\lambda = 0$ in Eq. (20), the dashed line to $\lambda = 0.6$, the long-dashed line to $\lambda = 0.8$, and the solid line to $\lambda = 1$. Data are from the compilation of Ref. [25].

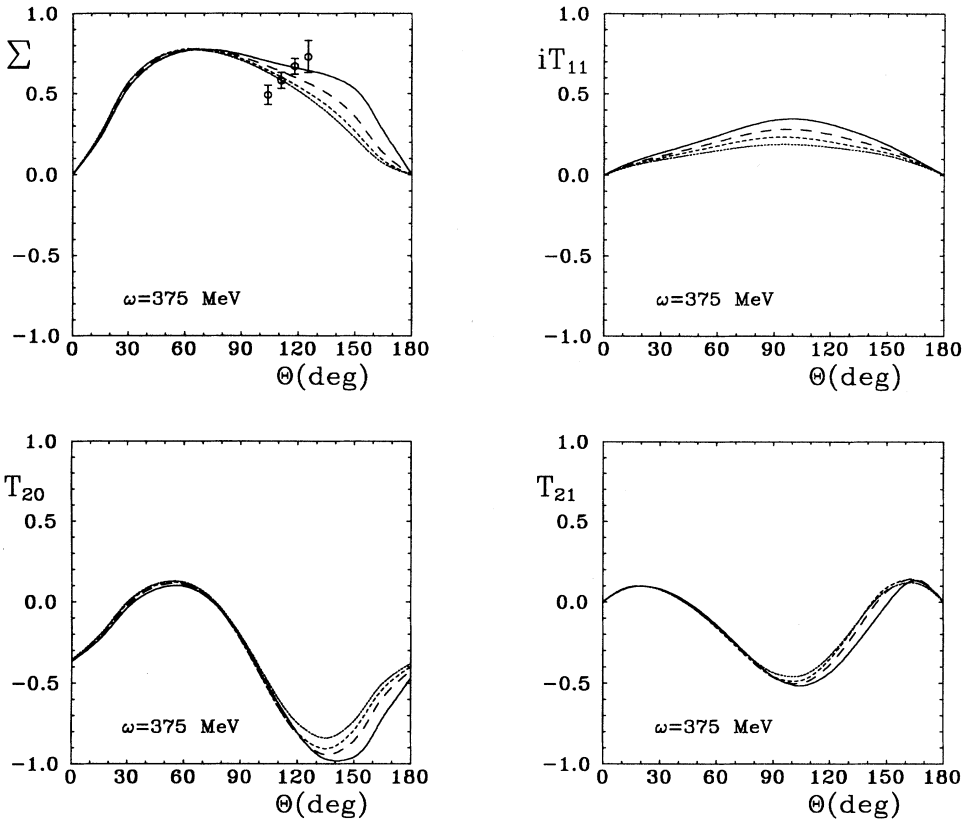

FIG. 9. Polarization observables of the $\gamma d \rightarrow \pi^0 d$ reaction at 375 MeV. The meaning of the curves is the same as in Fig. 8. Data are from the compilation of Ref. [25].

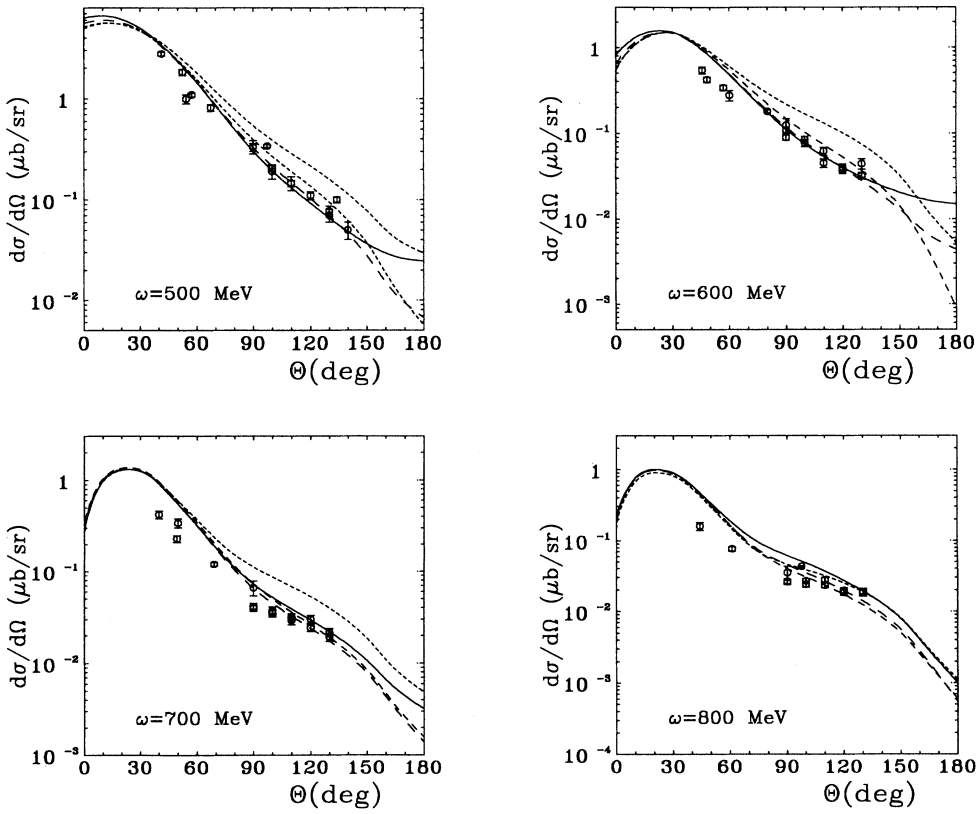

FIG. 10. Differential cross sections of the $\gamma d \rightarrow \pi^0 d$ reaction at 500, 600, 700, and 800 MeV. The meaning of the curves is the same as in Fig. 8. Data are from the compilation of Ref. [25].

that goes from around 10–20 % in the forward direction to as much as 50–100 % in the backward direction.

Very few data are available for polarization observables in this energy region. We show in Fig. 9 as an example of polarization observables the photon asymmetry Σ, the deuteron vector analyzing power iT_{11}, and the deuteron tensor analyzing powers T_{20} and T_{21} at 375 MeV. We have used here the same four values of λ as in the previous figure. The comparison with the available data for Σ is reasonably good, but clearly one cannot distinguish between the various models. The polarization observables, at this energy, are not very sensitive to the value of λ.

D. Second resonance region

We show in Fig. 10 the results for the differential cross section at 500, 600, 700, and 800 MeV. In this energy region there is similar sensitivity to the value of λ as observed in the region of the first resonance. Again in this case the models with λ large, and particularly the one with $\lambda = 0.8$, describe better the data. The results of the models with $\lambda = 0.2$ and 0.4, which are not shown, lie in between those of $\lambda = 0$ (short-dashed lines) and $\lambda = 0.6$ (dashed lines). The effects of the double-scattering term in this energy region are less than 20% for the angles where data are available.

We show in Fig. 11 the polarization observables Σ, iT_{11}, T_{20}, and T_{21} at 600 MeV. Unlike the results of Fig. 9, the polarization observables in this energy region are very sensitive to the parameter λ. A few data points are available for the photon asymmetry Σ, but with regard to the deuteron polarization observables, there are no data whatsoever.

E. Results at a fixed angle

A reasonably good amount of data exist in the form of excitation functions, that is, at a fixed angle and as functions of energy. This is particularly true for differential cross sections, but also to some extent for the photon asymmetry Σ. In a previous work [2], we have presented our results for $d\sigma/d\Omega$ and Σ at $\theta = 130°$ for energies between 400 and 900 MeV.

We start by showing in Fig. 12 our results for the differential cross section at $\theta = 90°$, 100°, 110°, and 120° for energies between 200 and 1000 MeV. The same four values of λ have been used as in the previous figures. The most striking feature of this figure is the strong sensitivity of the theoretical results on the parameter λ in the energy region of the Roper resonance (between 600 and 700 MeV), an effect already noticed in Ref. [2]. As seen from this figure, for energies up to about 800 MeV the data are clearly consistent with $\lambda = 0.8$. The fact that the $\lambda = 0.8$ model fails above 800 MeV is of no relevance, since as pointed out in Ref. [1] our model of the elementary $\gamma N \to \pi N$ amplitude is only valid up to about 800 MeV.

We show in Fig. 13 the differential cross section and photon asymmetry at $\theta = 130°$ and the remaining

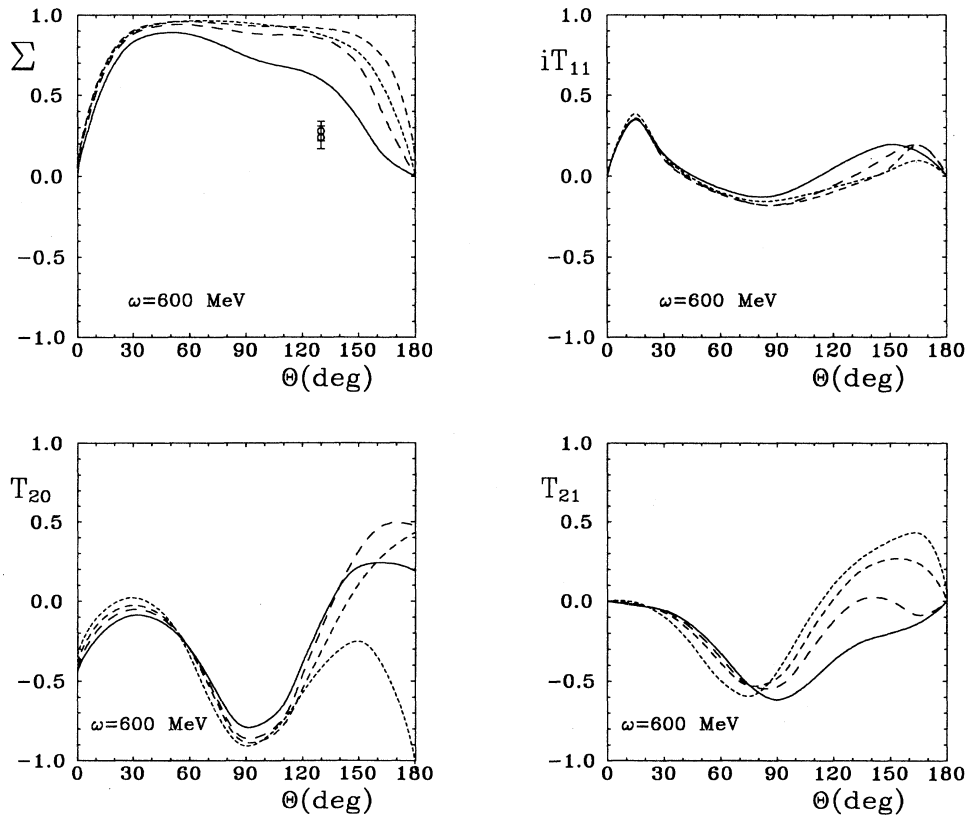

FIG. 11. Polarization observables of the $\gamma d \to \pi^0 d$ reaction at 600 MeV. The meaning of the curves is the same as in Fig. 8. Data are from the compilation of Ref. [25].

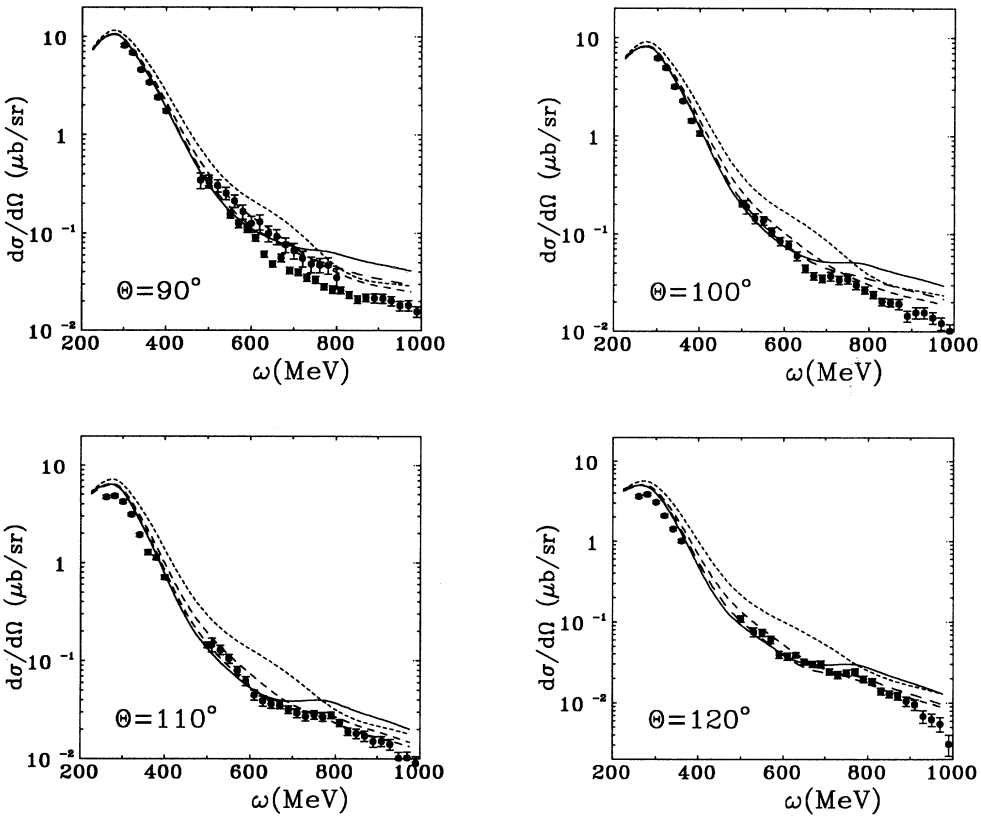

FIG. 12. Differential cross sections of the $\gamma d \rightarrow \pi^0 d$ reaction at $\theta = 90°$, 100°, 110°, and 120° as functions of energy. The meaning of the curves is the same as in Fig. 8. Data are from the compilation of Ref. [25].

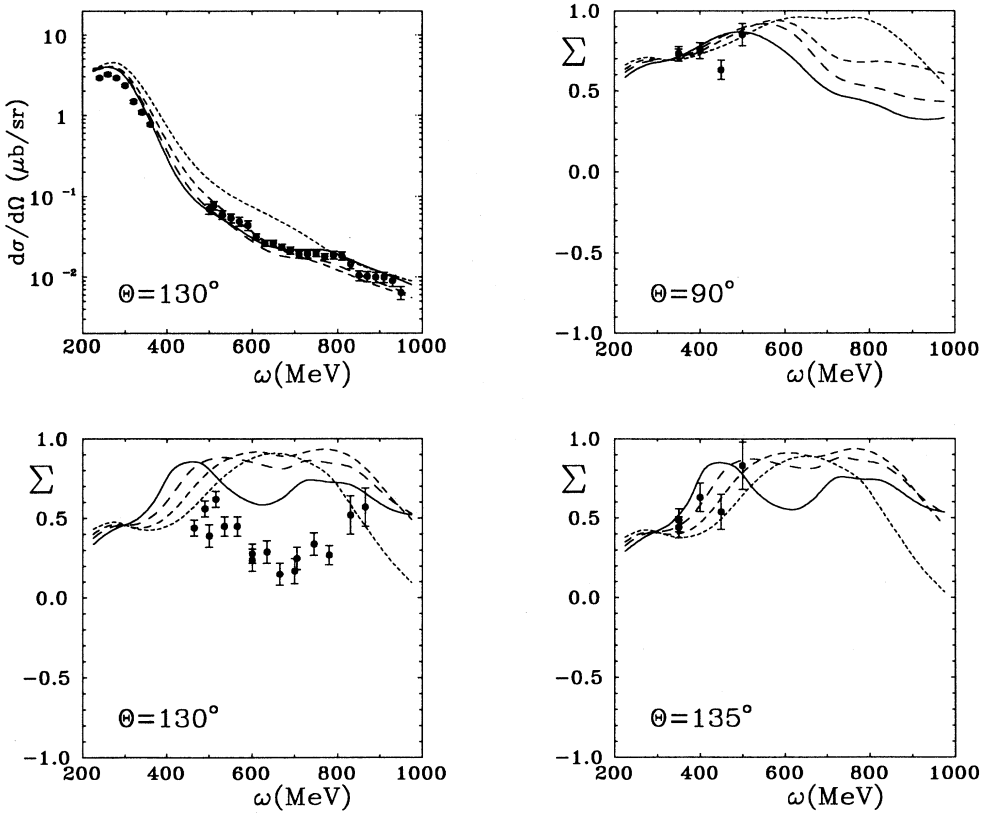

FIG. 13. Differential cross section and photon asymmetry of the $\gamma d \rightarrow \pi^0 d$ reaction at $\theta = 130°$ as functions of energy. Also shown are the photon asymmetry at $\theta = 90°$ and 135° as functions of energy. The meaning of the curves is the same as in Fig. 8. Data are from the compilation of Ref. [25].

photon-asymmetry data available at 90° and 135°. The differential cross section at $\theta = 130°$ is very well described up to 800 MeV by the model with $\lambda = 0.8$. With regard to the photon asymmetry at $\theta = 130°$, the model with $\lambda = 1$ describes the data better. The photon-asymmetry data at $\theta = 90°$ and 135° are restricted to energies below 500 MeV and they are consistent with all four theoretical models.

An interesting result of our calculation, which was already pointed out in Ref. [2], is the fact that the strong sensitivity with respect to the type of πNN coupling originates almost entirely from the deuteron wave function.

IV. CONCLUSION

We have performed a relativistic calculation of the reaction $\gamma d \to \pi^0 d$ taking into account the single- and double-scattering diagrams. Our model was applied at threshold and in the first and second resonance regions, in order to study the dependence of the observables on the form of the πNN vertex. The calculated results were compared with available data for the differential cross section and for the photon asymmetry, and predictions were presented for the vector and tensor analyzing powers of the deuteron. From our results in the threshold region, we concluded that the inclusion of the single- and double-scattering terms alone does not suffice to understand the data at threshold and a full three-body calculation is required there. In the first resonance region, the data seem to favor the models with λ large which correspond to a πNN vertex of predominantly pseudoscalar nature. In the region of the second resonance, the sensitivity with respect to the form of the πNN vertex is similar and the best description of the data was obtained with the $\lambda = 0.8$ model.

ACKNOWLEDGMENTS

We would like to thank Prof. F. Gross for valuable information concerning the Buck-Gross models. This work has been supported in part by DGICYT (Spain) under Contract No. PB870311. One of us (H.G.) would like to thank the Dirección General de Investigación Científica y Técnica of the Spanish Ministry for Science and Education for financial support (Ref. No. SAB92-0146). This work was supported in part (H.G.) by COFAA-IPN (Mexico).

[1] H. Garcilazo and E. Moya de Guerra, Nucl. Phys. **A562**, 521 (1993).
[2] H. Garcilazo and E. Moya de Guerra, Phys. Rev. C **49**, R601 (1994).
[3] M. T. Peña, H. Garcilazo, U. Oelfke, and P. U. Sauer, Phys. Rev. C **45**, 1487 (1992).
[4] P. Bosted and J. M. Laget, Nucl. Phys. **A296**, 413 (1978).
[5] C. Lazard, R. J. Lombard, and T. Maric, Nucl. Phys. **A271**, 317 (1977).
[6] P. Osland and A. K. Rej, Nuovo Cimento A **32**, 469 (1977).
[7] J. H. Koch and R. M. Woloshyn, Phys. Lett. **60B**, 221 (1977).
[8] J. H. Koch and R. M. Woloshyn, Phys. Rev. C **16**, 1968 (1977).
[9] J. D. Bjorken and S. D. Drell, *Relativistic Quantum Mechanics* (McGraw-Hill, New York, 1964).
[10] H. Garcilazo, Phys. Rev. C **35**, 1804 (1987).
[11] R. Blankenbecler and L. F. Cook, Phys. Rev. **119**, 1745 (1960).
[12] R. G. Arnold, C. E. Carlson, and F. Gross, Phys. Rev. C **21**, 1426 (1980).
[13] W. W. Buck and F. Gross, Phys. Rev. D **20**, 2361 (1979).
[14] F. Gross, Phys. Rev. D **10**, 223 (1974).
[15] J. Friar, Ann. Phys. (N.Y.) **104**, 380 (1977).
[16] R. D. Peccei, Phys. Rev. **176**, 1812 (1968).
[17] R. D. Peccei, Phys. Rev. **181**, 1902 (1969).
[18] Particle Data Group, J. J. Hernandez *et al.*, Phys. Lett. B **239**, 1 (1990).
[19] R. A. Ardnt, R. L. Workman, Z. Li, and L. D. Roper, Phys. Rev. C **42**, 1864 (1990).
[20] J. Adam, Jr. and E. Truhlik, Czech. J. Phys. B **34**, 1157 (1984).
[21] A. M. Bernstein and R. B. Holstein, Comments Nucl. Part. Phys. **20**, 197 (1991).
[22] I. Blomqvist and J. M. Laget, Nucl. Phys. **A280**, 405 (1977).
[23] M. G. Olsson and E. T. Osypowski, Nucl. Phys. **B87**, 399 (1975).
[24] P. Argan *et al.*, Phys. Lett. B **206**, 4 (1988); J. C. Bergstrom, in *Proceedings of the VII Miniconference on Electromagnetic Production of Mesons on Nucleons and Nuclei*, Amsterdam, 1991, edited by H. P. Blok, J. H. Koch, and H. de Vries (NIKHEF, Amsterdam, 1992), pp. 22–44.
[25] K. Ukai and T. Nakamura, Institute for Nuclear Study, University of Tokyo, Japan, Report No. INS-TEC-22, 1985.